Pressure and temperature-dependent quantum yields for the photodissociation of acetone between 279 and 327.5 nm

M. A. Blitz, D. E. Heard, and M. J. Pilling
Department of Chemistry, University of Leeds, Leeds, UK

S. R. Arnold and M. P. Chipperfield
School of the Environment, University of Leeds, Leeds, UK

Received 8 October 2003; revised 11 November 2003; accepted 16 February 2004; published 20 March 2004.

[1] The photodissociation of acetone has been studied over the wavelength (λ) range 279–327.5 nm as a function of temperature (T) and pressure (p) using a spectroscopic method to monitor the acetyl (CH_3CO) radical fragment. Above 310 nm the quantum yield (QY) is substantially smaller than previous measurements, and decreases with T. The QYs for production of $CH_3CO + CH_3$ and $CH_3 + CH_3 + CO$ have been parameterised as a function of λ, p and T and used to calculate the altitude dependence of the photolysis frequency. In the upper troposphere (UT) the acetone photolysis lifetime is a factor of 2.5–10 longer, dependent upon latitude and season, than if the previously recommended QYs are used. *INDEX TERMS:* 0317 Atmospheric Composition and Structure: Chemical kinetic and photochemical properties; 0322 Atmospheric Composition and Structure: Constituent sources and sinks; 0345 Atmospheric Composition and Structure: Pollution—urban and regional (0305); 0365 Atmospheric Composition and Structure: Troposphere—composition and chemistry. **Citation:** Blitz, M. A., D. E. Heard, M. J. Pilling, S. R. Arnold, and M. P. Chipperfield (2004), Pressure and temperature-dependent quantum yields for the photodissociation of acetone between 279 and 327.5 nm, *Geophys. Res. Lett.*, *31*, L06111, doi:10.1029/2003GL018793.

1. Introduction

[2] Airborne field campaigns have shown acetone to be an abundant and ubiquitous species in the troposphere [*Singh et al.*, 2001]. Photolysis of acetone in the UT is believed to be an important source of HO_x radicals and peroxyacetylnitrate (PAN), and proceeds via two channels with different wavelength thresholds [*Atkinson et al.*, 2002] (see http://www.iupac-kinetic.ch.cam.ac.uk):

$$CH_3COCH_3 \rightarrow CH_3CO + CH_3 \quad \lambda_{threshold} = 338\,nm \qquad (1)$$

$$CH_3COCH_3 \rightarrow CH_3 + CH_3 + CO \quad \lambda_{threshold} = 299\,nm \qquad (2)$$

The first channel dominates under tropospheric conditions. Inclusion of acetone photolysis has improved the agreement between measured and modelled UT concentrations of OH and HO_2 [*Jaeglé et al.*, 2001]. Previous measurements of the QY for acetone photolysis under atmospheric conditions have used gas chromatographic methods to monitor the loss of acetone or the build up of stable products, formed as a result of several reactions of the primary photofragments. *Gierczak et al.* [1998] monitored the loss of acetone and the production of CO_2 to determine the QY in air between 248–337 nm. A p dependence was observed above 270 nm but with almost no T dependence. *Emrich and Warneck* [2000] measured PAN QYs between 280–330 nm at 298 K formed through the scavenging of the $CH_3CO(O_2)$ radical by the addition of NO_2, and found similar results. *Warneck* [2001] used the results of both studies to derive a parameterisation that is recommended by IUPAC [*Atkinson et al.*, 2002]. In this work we use the OH radical, formed as a minor product of the reaction between CH_3CO and O_2 [*Blitz et al.*, 2002; *Tyndall et al.*, 1997]:

$$CH_3CO + O_2 + M \rightarrow CH_3CO(O_2) + M \qquad (3a)$$

$$CH_3CO + O_2 \rightarrow OH + products \qquad (3b)$$

as a sensitive spectroscopic marker of the CH_3CO fragment. We have measured the acetone photodissociation QY over a wide range of λ, p and T.

2. Experimental

[3] The apparatus uses laser-flash photolysis combined with laser-induced fluorescence (LIF), and has been described previously [*Blitz et al.*, 2002]. Acetone was photolysed using an excimer laser operating at 248 nm or a frequency-doubled pulsed tunable dye laser covering the λ range 279–327.5 nm, generating $[CH_3CO] \leq 10^{11}$ molecules cm^{-3}. The OH produced by reaction (3b) was probed by LIF at 282 nm using a second dye laser, with a detection limit $\leq 10^8$ molecule cm^{-3}. The two photolysis lasers counter-propagated through the photolysis cell (one or the other was blocked in a given experiment) at right-angles to the probe laser. Care was taken to ensure that the spatial overlap between the two photolysis lasers and the probe laser was identical for all experiments. The pulse repetition frequency of the lasers was 5 Hz, and the total flow of gas ensured there was a fresh sample of gas for each laser shot. A small concentration of acetone (6 Pa) was photolysed in the presence of varying pressures of He (0.6–540 hPa), N_2 (0.6–133 hPa) or air (0.6–80 hPa) in a T-controlled cell (218–295 K, ±1K). For the experiments involving He and N_2, a small amount of O_2 (13 Pa) was

0094-8276/04/2003GL018793$05.00

added to ensure rapid conversion of CH_3CO into OH via reaction (3b).

3. Determination of Photolysis Quantum Yields

[4] The kinetics of OH formation from reaction (3b) were measured as a function of p and T to demonstrate unequivocally that this reaction is the sole source of OH in our system and can be used as a marker for CH_3CO [*Blitz et al.*, 2002]. The rate coefficients were in excellent agreement with the literature [*Tyndall et al.*, 1997], and the OH yield from CH_3CO+O_2, denoted by α, was determined between 1–400 Torr for 213 and 295 K. For 295 K, $\alpha = 1$ and 0.09 at 1 and 400 Torr, respectively, dropping at higher p due to increased competition from channel (3a) to form the adduct $CH_3CO(O_2)$.

[5] The acetone photolysis QY at a chosen λ was obtained as follows. For a given p and T, the rise of OH was recorded by changing the delay time between the pump and probe lasers. OH formed in reaction (3b) is removed slowly either by reaction with acetone or by diffusion. A bi-exponential function was fitted to the OH temporal behaviour, from which a relative value of $\alpha[CH_3CO]_{0,\lambda}$ was obtained, where $[CH_3CO]_{0,\lambda}$ is the initial concentration of CH_3CO. The experiment was then repeated (always within 5 minutes) at a photolysis λ of 248 nm, and the OH profile again measured and fitted to obtain $\alpha[CH_3CO]_{0,248}$, ensuring that the spatial overlap between the photolysis and probe lasers at the laser-excitation region was kept identical. The $[CH_3CO]_0$ ratio at λ and 248 nm is linked to the acetone photolysis yields via:

$$\frac{[CH_3CO]_{0,\lambda}}{[CH_3CO]_{0,248}} = \frac{N_\lambda}{N_{248}} \frac{\sigma_\lambda}{\sigma_{248}} \frac{\phi_{CH_3CO,\lambda}}{\phi_{CH_3CO,248}} \quad (4)$$

where N_λ is the number of photons per laser pulse, (determined from an average of $\geq$50 shots), and σ_λ is the T-dependent acetone absorption cross-section, measured between 235 and 298 K by *Gierczak et al.* [1998]. N_λ was chosen to give approximately the same $[CH_3CO]_0$ at low p, and hence OH signal, as observed at 248 nm. The OH yield, α, and the degree of quenching of the OH fluorescence for a given p are the same at the two wavelengths, and so cancel in equation (4) above and are not required. The degree of excitation within the initially formed acetyl radical will change with λ, but at the total pressures used here, the acetyl fragment will be relaxed rapidly and α is not expected to change with λ. A measurement of a pair of OH profiles enables a value of $\frac{\phi_{CH_3CO,\lambda}}{\phi_{CH_3CO,248}}$ to be calculated and, as $\phi_{CH_3CO,248}$ is independent of p [*Gierczak et al.*, 1998], the p dependence of $\phi_{CH_3CO,\lambda}$ can conveniently be analysed using a Stern-Volmer relationship:

$$\frac{\phi_{CH_3CO,248}}{\phi_{CH_3CO,\lambda}} = \left(\frac{\phi_{CH_3CO,248}}{\phi_{CH_3CO,\lambda}}\right)_{[M]=0} (1 + A_1[M]) \quad (5)$$

A plot of $\frac{\phi_{CH_3CO,248}}{\phi_{CH_3CO,\lambda}}$ versus $[M]$ has an intercept $I(\lambda) = \left(\frac{\phi_{CH_3CO,248}}{\phi_{CH_3CO,\lambda}}\right)_{[M]=0}$ and a gradient proportional to A_1, a measure of the ratio k_M/k_D, where k_D and k_M are the rate coefficients for dissociation and collisional quenching of the excited singlet state of acetone, respectively. Equation (5) is a good representation of the data for $\lambda < 302$ nm at all p. However, for $\lambda \geq 302$ nm an extended form of the Stern-Volmer expression is necessary:

$$\frac{\phi_{CH_3CO,248}}{\phi_{CH_3CO,\lambda}} = \left(\frac{\phi_{CH_3CO,248}}{\phi_{CH_3CO,\lambda}}\right)_{[M]=0} (1 + A_2[M] + A_3) \frac{1 + A_4[M]}{1 + A_4[M] + A_3} \quad (6)$$

reflecting dissociation and quenching from both the singlet and triplet excited states of acetone. For $p > 2000$ Pa (15 Torr), the last term is $\sim$1 and equation (6) is linear in $[M]$, but for lower p the last term becomes dependent upon $[M]$ and equation (6) is non-linear. A more detailed discussion of the photophysics of acetone and the extended Stern-Volmer treatment will be the subject of a future publication (M. A. Blitz et al., manuscript in preparation, 2004).

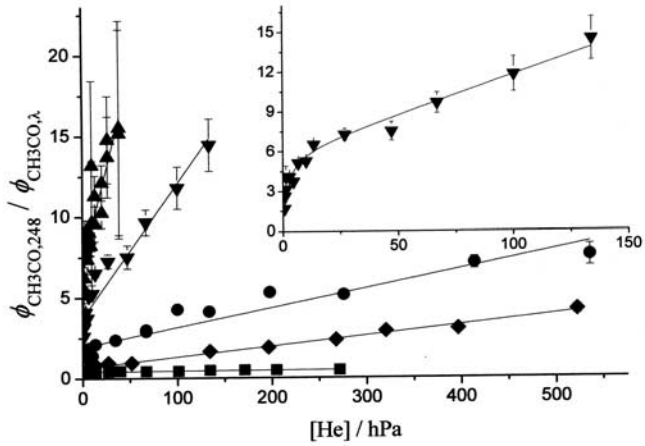

Figure 1. Stern-Volmer plots for 283 (squares), 309 (diamonds), 315 (circles), 322.5 (inverted triangles, and inset) and 327.5 nm (triangles) at 295 K for He buffer gas, with acetone = 6 Pa, O_2 = 13 Pa. The ordinate is the reciprocal of the acetyl radical yield relative to the value at the reference λ of 248 nm, together with 95% confidence limits. The solid lines are weighted least-squares fits of equation (5) (283 nm) or equation (6) (all other λ) to the data.

Figure 1 shows Stern-Volmer plots of $\frac{\phi_{CH_3CO,248}}{\phi_{CH_3CO,\lambda}}$ versus $[M]$ and best-fits of either equation (5) or (6) for a variety of photolysis λ. The ratio $\frac{\phi_{CH_3CO,248}}{\phi_{CH_3CO,\lambda}}$ increases at higher p due to the reduction in caused by collisional quenching of photoexcited acetone, and the gradient increases sharply above 300 nm as the value of k_D decreases rapidly [*Emrich and Warneck*, 2000]. For $\lambda < 300$ nm A_1 is small and $\phi_{CH_3CO,\lambda}$ varies little with p, consistent with previous studies [*Gierczak et al.*, 1998; *Warneck*, 2001]. The curvature at longer λ is clear, but the excellent fit of either equation (5) or (6) to the data allows accurate extrapolation up to $p = 1$ atm. At the limit $p = 0$ the total QY for acetone photolysis is given by:

$$(\phi_{total})_{[M]=0} = (\phi_{CH_3CO,\lambda})_{[M]=0} + \phi_{CO,\lambda} = \frac{\phi_{CH_3CO,248}}{I(\lambda)} + \phi_{CO,\lambda} = 1 \quad (7)$$

(the rate of fluorescence is negligible compared to that for dissociation) and hence $I(\lambda) = \frac{\phi_{CH_3CO,248}}{1-\phi_{CO,\lambda}}$. Previous studies

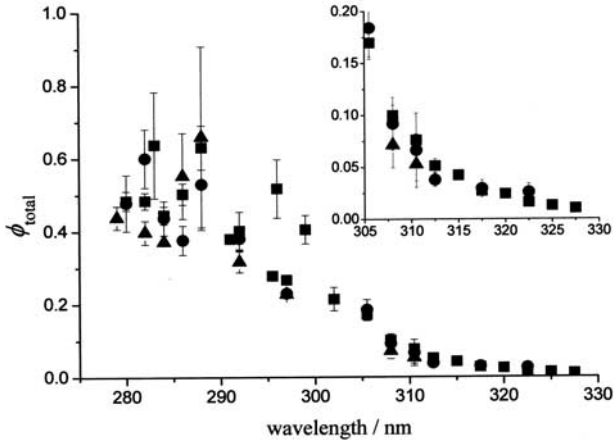

Figure 2. Total QY at 295K for He (squares, 13 Pa O_2) N_2 (circles, 13 Pa O_2) and air (triangles) buffer gas for a p of 1 atm (1000 hPa), obtained from fits to individual Stern-Volmer plots, with 95% confidence limits.

have shown that $\phi_{CO,\lambda}$, the yield of CO via channel (2), is independent of p [*Gandini and Hackett*, 1977; *Horowitz*, 1991], and a further discussion of this is given in M. A. Blitz et al. (manuscript in preparation, 2004). At 248 nm, $(\phi_{CH_3CO,\lambda})_{[M]=0} = \phi_{CH_3CO,248}$ and hence $I(\lambda) = 1$, with $I(\lambda)$ decreasing with increasing λ to a limiting value of $\phi_{CH_3CO,248}$ at longer λ when $\phi_{CO,\lambda} \rightarrow 0$. A plot of $I(\lambda)$ versus λ gave $\phi_{CH_3CO,248} = 0.35$, and hence $\phi_{CO,248} = 0.65$ at 295 K. The value of $\phi_{CO,\lambda}$ at any other λ was obtained from the variation of $I(\lambda)$ with λ, and $(\phi_{CH_3CO,\lambda})_{[M]=0}$ from $1 - \phi_{CO,\lambda}$. Using the fits to the Stern-Volmer plots the value of $\phi_{CH_3CO,\lambda}$ at any p could then be calculated.

4. Quantum Yields as a Function of λ and T

[6] In total ~50 Stern-Volmer plots of the type shown in Figure 1, each containing data taken at ~20 pressures, were assembled for $\lambda = 279-327.5$ nm, $p = 0.66-540$ hPa (He, N_2 or air) and $T = 295$ K, 273 K, 248 K and 218 K. For a given λ and T, the values of $I(\lambda)$ and A_1 for $\lambda < 302$ nm, or $I(\lambda)$ and A_2, A_3, A_4 for $\lambda \geq 302$ nm, obtained from the fits for the 3 different buffer gases, did not show any systematic differences. Figure 2 shows $\phi_{total} = \phi_{CH_3CO,\lambda} + \phi_{CO,\lambda}$ for $\lambda = 279-327.5$ nm at T = 295K and $p = 1000$ hPa for the buffer gases He, N_2 and air. Although there is some scatter, no systematic difference was found between the collision partners. The precise mechanism for collisional quenching of excited acetone is uncertain (M. A. Blitz et al., manuscript in preparation, 2004), but our data suggest all gases quench with similar efficiency. While the precision of individual experiments is very high, the reproducibility is limited by the difficulty in maintaining constant overlap between three laser beams or the calibration of the laser power over long periods.

[7] Figure 3 shows ϕ_{total} at 295 K together with the QYs determined by *Gierczak et al.* [1998], who either measured the loss of acetone (ϕ_{total}, $\lambda < 308$ nm only) or the production of CO_2 (giving ~20% less than ϕ_{total}, all λ), and by *Emrich and Warneck* [2000], who measured yields of PAN and hence $\phi_{CH_3CO,\lambda}$, for $p = 1$ atm and 295 K. The agreement is very good for $\lambda < 310$ nm, but at longer λ our measurements become significantly smaller. At 320 nm and 1 atm the yields are 0.024 (this work), 0.035 [*Gierczak et al.*, 1998] and 0.06 [*Emrich and Warneck*, 2000]. Our time-resolved experiments are more direct and sensitive than previous studies using end-product analysis, and as they do not rely on a detailed knowledge of the reaction mechanism linking the photolysis event to observed products, may be less subject to interferences.

[8] The T dependence of ϕ_{total} for $\lambda = 280-327.5$ nm is shown in Figure 4 for a constant density of 5×10^{18} molecule cm^{-3} (150 hPa at 218 K, typical of the UT). The T dependence of ϕ_{total} below 295 nm is small, and similar to the scatter in the data, but at longer λ is quite striking, with ϕ_{total} (295 K)/ϕ_{total} (218 K) ~4 and ~20 at 310 nm and 322.5 nm, respectively. The data shown are for He buffer gas, but points recorded for M = N_2 and air at selected λ and T showed no systematic difference in QYs. In contrast, at 308 nm *Gierczak et al.* [1998] found a T-independent yield between 298 and 195 K for a given gas density, as recommended by IUPAC [*Atkinson et al.*, 2002].

5. Parameterisation of Quantum Yields for Atmospheric Modelling

[9] It was not possible to find a single parameterisation to adequately represent the QY for all λ so two regions were used. For $\lambda = 279-302$ nm, equation (5) was fitted globally to all the Stern-Volmer plots at the four temperatures studied, using a least-squares routine to minimise χ^2, the goodness of fit. The error for each individual point on the Stern-Volmer plots was used to weight the fit. For $\lambda = 302-327.5$ nm, a similar routine was used, except equation (6) for the extended Stern-Volmer analysis was fitted to all the data. The optimised parameterisation is as follows:

$$\phi_{total}(\lambda, [M], T) = \phi_{CH_3CO}(\lambda, [M], T) + \phi_{CO}(\lambda, T) \qquad (8)$$

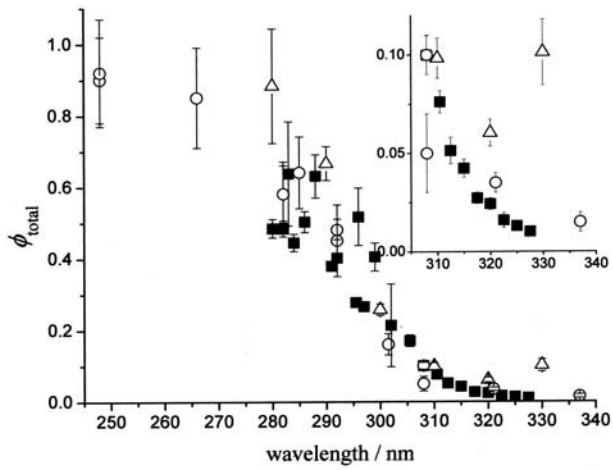

Figure 3. Total QY at 1 atm (1000 hPa) and 295 K determined in this work from fits to individual Stern-Volmer plots (squares), by *Gierczak et al.* [1998] (circles), and by *Emrich and Warneck* [2000] (triangles).

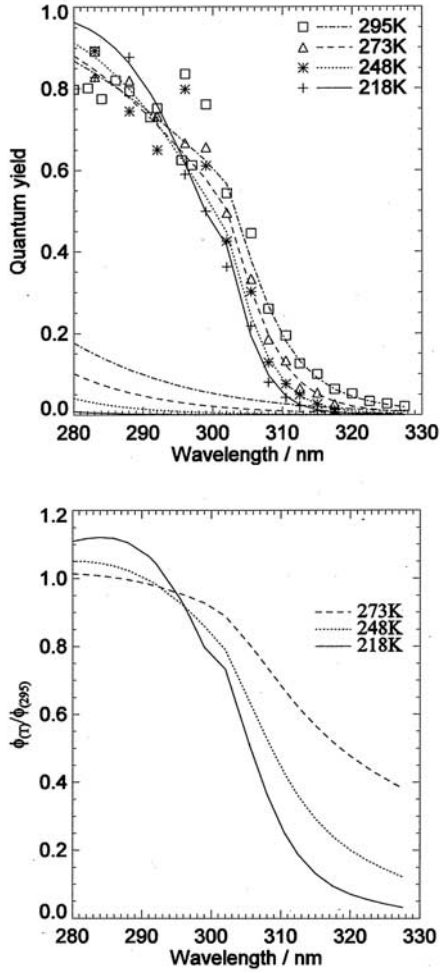

Figure 4. (top) Total measured QY (symbols) and parameterised forms of ϕ_{total} and ϕ_{CO} calculated using equations (8)–(11) as a function of T for [M] = 5×10^{18} molecule cm^{-3}. (bottom) ϕ_{total} (T)/ϕ_{total} (295 K).

For λ = 279–327.5 nm, the CO yield is assumed independent of [M], and is given by:

$$\phi_{CO}(\lambda, T) = \frac{1}{1 + A_0} \tag{9}$$

$$A_0 = \frac{a_0}{1 - a_0} \exp[b_0\{\lambda - 248\}]$$

$$a_0 = (0.350 \pm 0.003)(T/295)^{(-1.28\pm0.03)}$$

$$b_0 = (0.068 \pm 0.002)(T/295)^{(-2.65\pm0.20)}$$

For λ = 279–302 nm

$$\phi_{CH_3CO}(\lambda, [M], T) = \frac{1 - \phi_{CO}(\lambda, T)}{1 + A_1[M]} \tag{10}$$

$$A_1 = a_1 \exp\left[-b_1\left\{\left(10^7/\lambda\right) - 33113\right\}\right]$$

$$a_1 = (1.600 \pm 0.032) \times 10^{-19}(T/295)^{(-2.38\pm0.08)}$$

$$b_1 = (0.55 \pm 0.02) \times 10^{-3}(T/295)^{(-3.19\pm0.13)}$$

For λ = 302–327.5 nm

$$\phi_{CH_3CO}(\lambda, [M], T) = \frac{(1 + A_4[M] + A_3)}{(1 + A_2[M] + A_3)(1 + A_4[M])} \cdot (1 - \phi_{CO}(\lambda, T)) \tag{11}$$

$$A_2 = a_2 \exp\left[-b_2\left\{\left(10^7/\lambda\right) - 30488\right\}\right]$$

$$a_2 = (1.62 \pm 0.06) \times 10^{-17}(T/295)^{(-10.03\pm0.20)}$$

$$b_2 = (1.79 \pm 0.02) \times 10^{-3}(T/295)^{(-1.364\pm0.036)}$$

$$A_3 = a_3 \exp\left[-b_3\left\{\frac{10^7}{\lambda} - c_3\right\}^2\right]$$

$$a_3 = (26.29 \pm 0.88)(T/295)^{(-6.59\pm0.23)}$$

$$b_3 = (5.72 \pm 0.20) \times 10^{-7}(T/295)^{(-2.93\pm0.09)}$$

$$c_3 = (30006 \pm 41)(T/295)^{(-0.064\pm0.004)}$$

$$A_4 = a_4 \exp\left[-b_4\left\{\left(10^7/\lambda\right) - 30488\right\}\right]$$

$$a_4 = (1.67 \pm 0.14) \times 10^{-15}(T/295)^{(-7.25\pm0.54)}$$

$$b_4 = (2.08 \pm 0.07) \times 10^{-3}(T/295)^{(-1.16\pm0.15)}$$

where in all cases the units are [M] (molecule cm^{-3}), λ (nm) and T (K). In the limit of [M] = 0, ϕ_{CH_3CO} (λ, [M], T) = 1 − ϕ_{CO}(λ, T). The parameterisation is valid for 218–295 K, and for p up to 1000 hPa. The error bars for each parameter represent 95% confidence limits, and are propagated errors from the global fit. The overall error in the parameterised curve is 10–15%.

[10] Figure 4 also shows the variation with λ of the parameterised forms of ϕ_{total} and ϕ_{CO} for T = 295, 273, 248 and 218 K, and for constant [M] = 5×10^{18} molecule cm^{-3}. ϕ_{CO} is small in this region, and decreases rapidly with T. The slight discontinuity in the parameterised curve at 302 nm is caused by the switch-over from equations (10)–(11) to describe ϕ_{CH_3CO}.

6. Variation of Acetone Photolysis With Altitude

[11] The atmospheric photolysis rate of acetone is given by:

$$J = \int_{\lambda} \sigma(\lambda, T)\phi_{total}(\lambda, [M], T)F(\lambda, z, \chi)d\lambda \tag{12}$$

where F is the actinic photon flux that depends upon altitude, z, and solar zenith angle, χ. The CiTTyCAT box

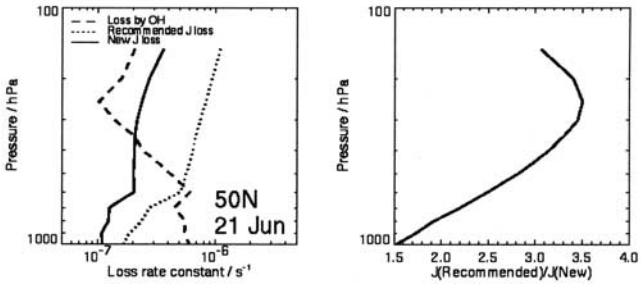

Figure 5. (left) Rate of loss of acetone by photolysis and reaction with OH calculated as a function of altitude for 21 June at 50°N. (right) Ratio *J*(Recommended)/*J*(New).

model [*Evans et al.*, 2000] was used to calculate the diurnally averaged acetone loss rates due to reaction with OH and photolysis over a range of 13 levels in a column from 1000 hPa to 150 hPa. Figure 5 shows *J*(New) calculated for 21 June at latitude 50°N using the parameterised form of $\phi_{total}(\lambda, [M], T)$ given above, together with the rate of loss of acetone by reaction with OH, using rate constants recommended by IUPAC. Temperature was taken from the US Standard Atmosphere (1976), O_3 and CH_4 were from a 2-D model [*Law and Pyle*, 1993] and H_2O was the saturated vapour pressure at each model level. The acetone absorption cross sections ($\sigma(\lambda, T)$) were taken from *Gierczak et al.* [1998]. Figure 5 also shows *J*(Recommended) calculated using acetone photolysis yields recommended by IUPAC and the ratio *J*(Recommended)/*J*(New). The photolysis rate is significantly slower at all *z* if the new QY are used, being a factor of 3.5 lower in the UT/lower stratosphere region. The effect is more pronounced at higher *z* because the new QY drop off sharply at the lower *T* (see Figure 4). The altitude at which photolysis begins to dominate the acetone loss increases significantly when the new QY are used. The reduction in *J* using the new QY is slightly less pronounced at 0°N for overhead sun (21 March, factor of 2.65 at 200 hPa), but for 50°N in mid-winter (21 December), *J* is reduced by a factor of 10 at 200 hPa, and a factor of 3 at the surface (see auxiliary material[1]). Further atmospheric implications of the new *T*-dependent QY for acetone will be discussed in *Arnold* [2004].

7. Summary

[12] A new method to monitor CH_3CO has been used to measure the QY for both photodissociation channels of acetone between 279–327.5 nm as a function of *T* and *p*. In contrast to previous studies, the QY was observed to decrease significantly at lower *T*, being significantly smaller (e.g., for 320 nm, 218 K, 150 hPa, by a factor of ~20) than currently recommended values. From data recorded at ~1000 combinations of *T*, *p* and λ, two parameterised forms of the photodissociation QY were determined for λ below and above 302 nm, and used to calculate acetone photolysis rates as a function of altitude. The new QY show photolysis to be a less important sink for acetone, compared to recommended values, especially in the colder UT region, with important implications for its budget and associated chemistry.

[13] **Acknowledgments.** MAB, DEH and MJP thank the NERC UTLS-O3 programme (award GST/02/2428) for funding this work.

References

Arnold, S. R., M. P. Chipperfield, M. A. Blitz, D. E. Heard, and M. J. Pilling (2004), Photodissociation of acetone: Atmospheric implications of temperature-dependent quantum yields, *J. Geophys. Res.*, doi:10.1029/2001JA900021, in press.

Atkinson, R., et al. (2002), Summary of evaluated kinetic and photochemical data for atmospheric chemistry, *Data Sheet P7*, Int. Union of Pure and Appl. Phys., London.

Blitz, M. A., D. E. Heard, and M. J. Pilling (2002), OH formation from CH_3CO+O_2: A convenient experimental marker for the acetyl radical, *Chem. Phys. Lett.*, *365*, 374–379.

Emrich, M., and P. Warneck (2000), Photodissociation of acetone in air: Dependence on pressure and wavelength. Behavior of the excited singlet state, *J. Phys. Chem. A*, *104*, 9436–9442.

Evans, M. J., et al. (2000), Evaluation of a Lagrangian box model using field measurements from EASE (Eastern Atlantic Summer Experiment) 1996, *Atmos. Environ.*, *34*, 3843–3863.

Gandini, A., and P. A. Hackett (1977), Electronic relaxation processes in acetone and 1, 1, 1-trifluoroacetone vapour and the gas phase recombination of the acetyl radical at 22°C, *J. Am. Chem. Soc.*, *99*, 6195–6205.

Gierczak, T., et al. (1998), Photochemistry of acetone under tropospheric conditions, *Chem. Phys.*, *231*, 229–244.

Horowitz, A. (1991), Wavelength dependence of the primary photodissociation processes in acetone photolysis, *J. Phys. Chem.*, *95*, 10,816–10,823.

Jaeglé, L., et al. (2001), Chemistry of HOx radicals in the upper troposphere, *Atmos. Environ.*, *25*, 469–489.

Law, K. S., and J. A. Pyle (1993), Modeling trace gas budgets in the troposphere: 1. Ozone and odd nitrogen, *J. Geophys. Res.*, *98*, 18,377–18,400.

Singh, H., et al. (2001), Evidence from the Pacific troposphere for large global sources of oxygenated organic compounds, *Nature*, *410*, 1078–1081.

Tyndall, G. S., et al. (1997), Pressure dependence of the rate coefficients and product yields for the reaction of CH_3CO radicals with O_2, *Int. J. Chem. Kinet.*, *29*, 655–663.

Warneck, P. (2001), Photodissociation of acetone in the troposphere: An algorithm for the quantum yield, *Atmos. Environ.*, *35*, 5773–5777.

[1]Auxiliary material is available at ftp://ftp.agu.org/apend/gl/2003GL018793.

S. R. Arnold and M. P. Chipperfield, School of the Environment, University of Leeds, Leeds LS2 9JT, UK.

M. A. Blitz, D. E. Heard, and M. J. Pilling, Department of Chemistry, University of Leeds, Leeds LS2 9JT, UK. (dwayneh@chem.leeds.ac.uk)